Ratiometric fluorescent nanosensors for selective detecting cysteine with upconversion luminescence

Article *in* Biosensors & Bioelectronics · September 2015

DOI: 10.1016/j.bios.2015.09.034

CITATIONS
11

READS
56

6 authors, including:

Bin Li
Chinese Academy of Sciences
297 PUBLICATIONS **4,059** CITATIONS
SEE PROFILE

Ma Heping
Changchun Institute of Optics, Fine Mechani…
28 PUBLICATIONS **504** CITATIONS
SEE PROFILE

Biosensors and Bioelectronics 77 (2016) 124–130

Contents lists available at ScienceDirect

Biosensors and Bioelectronics

journal homepage: www.elsevier.com/locate/bios

Ratiometric fluorescent nanosensors for selective detecting cysteine with upconversion luminescence

Yunlong Guan [a,b], Songnan Qu [a], Bin Li [a,*], Liming Zhang [a], Heping Ma [a], Ligong Zhang [a]

[a] State Key Laboratory of Luminescence and Applications, Changchun Institute of Optics Fine Mechanics and Physics, Chinese Academy of Sciences, Changchun 130033, PR China
[b] University of Chinese Academy of Sciences, Beijing 100039, PR China

ARTICLE INFO

Article history:
Received 9 June 2015
Received in revised form
2 September 2015
Accepted 14 September 2015
Available online 16 September 2015

Keywords:
Cysteine
Fluorescence
Nanosensor
Upconversion
Mesoporous silica

ABSTRACT

Fluorescent sensors based on upconversion (UC) luminescence have been considered as a promising strategy to detect bio-analyte due to their advantages in deep penetration, minimum autofluorescence, and ratiometric fluorescent output. A prototype of nanosensors combined with mesoporous silica coated upconversion nanoparticles (UCNPs) and a fluorescein-based fluorescent probe loaded in pores was therefore designed to detect cysteine (Cys). The silica shell provided loading space for the probe and enabled the nanosensors to disperse in water. In the presence of Cys, the fluorescent probe was transformed into 5(6)-carboxyfluorescein with an emission band centering at 518 nm which was secondarily excited by the light at around 475 nm from NaYF4:Yb^{3+}, Tm^{3+} UCNPs driven by 980 nm near-infrared (NIR) laser. The intensity ratio between green and blue luminescence (I_{518}/I_{475}) grew exponentially with increasing concentrations of Cys over a range of 20–200 μmol L^{-1}. The response of the nanosensors towards Cys was recognizable with naked eyes by luminescence color change. Evidences suggest that these nanosensors are capable of sensing Cys in aqueous solution and distinguishing Cys from homocysteine (Hcy) with kinetically-controlled selectivity. The system was further employed to detect Cys in human serum and the result was in agreement with it tested by high performance liquid chromatography with acceptable recovery.

1. Introduction

Small biological thiols, as a class of molecules containing free thiol moiety, for instance cysteine (Cys), homocysteine (Hcy) and glutathione (GSH), are essential in many physiological processes (Reddie and Carroll 2008; Weerapana et al., 2010). Abnormal levels of thiols lead to a series of impairments. For instance, evidence indicates that a raised level of Hcy in serum is responsible for cardiovascular disease (Wald et al., 2002), and has an association with posttraumatic stress disorder (Levine et al., 2008). Plasma Hcy is reported a risk factor for dementia and Alzheimer's disease (Seshadri et al., 2002). Cys is a precursor to glutathione whose thiolate substituent is able to coordinate with varieties of metal ions including metal cofactors in enzymes, and harmful heavy metal ions like mercury, lead and cobalt to assist detoxification. Their levels are also crucial to metabolic equilibrium where diseases including slowed growth in children, depigmentation of hair, edema, lethargy, liver damage, loss of muscle and fat, skin lesions and weakness may be encountered upon its deficiency (Shahrokhian 2001). For these reasons, thiol determination in biological samples has a great importance in health monitoring and disease prediction.

It is efficient to detect bio-thiols with fluorescent chemosensors. Due to specific processes of chemical reactions, certain reaction-based fluorescent sensors exhibit favorable sensitivity and selectivity to thiols including Cys, Hcy and GSH (Chen et al., 2010; Peng et al., 2012). Some of them with subtle design can effectively distinguish Cys from Hcy and other thiols (Wang et al., 2012a, 2012b; Yuan et al., 2011). However, most organic-dye-based probes working in visible region need to be excited by UV light resulting in autofluorescence and photo damage, dye photobleaching and insufficient aqueous solubility. Modified upconversion nanoparticles (UCNPs) with hydrophilic surface, on the other hand, are believed to overcome such disadvantages. The excitation light for UCNPs is within the near-infrared (NIR) window of tissues. Therefore, the use of NIR light affords deeper penetration depth, lower autofluorescence and less photo damage in biological samples.

It is unpractical to detect analyte concentration using a fluorescent probe with single emission band without internal standard

* Corresponding author.
E-mail address: libinteacher@163.com (B. Li).

http://dx.doi.org/10.1016/j.bios.2015.09.034
0956-5663/

(Yuan et al. 2013). By using intensity ratio between two emission bands, ratiometric sensors improve sensing accuracy and reliability (Ding et al., 2013; Li et al., 2012, 2014; Liu et al., 2014, 2011; Yao et al., 2012; Zhang et al., 2013). Li and coworkers reported "yolk-shell" upconversion nanocomposites for sensing Cys/Hcy, which provided an efficient method to combine fluorescent probe with UCNPs (Zhao et al., 2014). Yet it is still difficult to distinguish Cys from Hcy with ratiometric upconversion sensors.

To selectively detect Cys concentration in aqueous environment, a prototype of nanosensors based on the emission–reabsorption process from UCNPs to fluorescent probes was designed in this work. A fluorescein-based reactive fluorescent probe 5(6)-carboxyfluorescein-O,O′-diacrylate (Probe 1) was synthesized and characterized (Wang et al., 2012b). These UCNPs were modified with mesoporous silica shell, so that Probe 1 was able to be loaded into them. Upon 980 nm laser exposure, the UCNPs emit blue light at around 475 nm which in turn excites Probe 1 to detect Cys in aqueous solution. While reacting with Cys, Probe 1 is transformed into 5(6)-carboxyfluorescein, showing green fluorescence centering at 518 nm. With advantages of sufficient water dispersity, improved selectivity, rapid response and ratiometric fluorescence, the system is anticipated to be a promising sensor for Cys.

2. Materials and methods

2.1. Chemicals and materials

Rare-earth oxides RE_2O_3 (99.99%; RE=Y, Yb, and Tm) were purchased from Science and Technology Parent Company of Changchun Institute of Applied Chemistry. Oleic acid (OA; >90%) and 1-octadecene (ODE; >90%) were purchased form Sigma-Aldrich. Acryloyl chloride, 5(6)-carboxyfluorescein, and amino acids were purchased form Aladdin. Tetraethyl orthosilicate (TEOS; AR) and Cetyltrimethylammonium bromide (CTAB; AR) were purchased from Sinopharm Chemical Regent Co., Ltd. All solvents were purchased from Beijing Chemical Works. Dichloromethane (CH_2Cl_2) was dried by refluxing with calcium hydride and used after distillation. Triethylamine (Et_3N) was dried with KOH and used after distillation. Other chemicals were used as received without further purifications. Human serum sample was collected from a 61 years old male volunteer in Jilin Province People's Hospital.

2.2. Characterization

Transmission electron microscopy (TEM) images were taken to visualize the prepared nanostructure with JEM-2010 (JEOL, Tokyo, Japan). Scanning electronic microscopy (SEM) images were recorded on a Hitachi S-4800 microscope. Energy dispersive spectra (EDS) were obtained on an EDAX Genesis module in conjunction with Hitachi S-4800 microscope. Powder X-ray diffraction (XRD) patterns were recorded on a Bruker D4 X-ray diffractometer (Germany) with Ni-filtered Cu K radiation (40 kV, 30 mA). Nitrogen adsorption and desorption isotherms were measured using a Nova 1000 analyzer. Surface areas were calculated by the Brunauer–Emmett–Teller (BET) method, the pore volume and pore size distributions were calculated using Barrett–Joyner–Halenda (BJH) model. All spectra of nanosensors was performed with samples dispersed in phosphate buffered saline (PBS, pH=7.4) in a quartz cell for measurement. All photoluminescence (PL) spectra were measured with a Hitachi F-4500 fluorescence spectrophotometer, a 980 nm CW laser was used as excitation source. Upconversion lifetime curves were obtained on a fluorescence lifetime measurement system with an optical parametric oscillator (OPO) as excitation source and a Tektronix digital oscilloscope (TDS 3052) as signal detector. High performance liquid chromatography (HPLC) was performed using Waters 600 instrument with a XAqua C18 5 μm 100 Å column and an Alltech ELSD 2000ES evaporative light-scattering detector (ELSD).

2.3. Synthesis of core–shell $NaYF_4$: Yb^{3+}, Tm^{3+} @$NaYF_4$ nanoparticles (UCNPs)

All rare-earth chlorides $RECl_3 \cdot 6H_2O$ (RE=Y, Yb, and Tm) were prepared by dissolving RE_2O_3 powder in hydrochloric acid. Hexagonal-phase core–shell $NaYF_4$:Yb^{3+}, Tm^{3+} @$NaYF_4$ was synthesized following a reported procedure with some modifications (Liu et al., 2014). 2 mmol of lanthanide chlorides (1.59 mmol $YCl_3 \cdot 6H_2O$, 0.40 mmol $YbCl_3 \cdot 6H_2O$ and 0.01 mmol $TmCl_3 \cdot 6H_2O$) were added into a 100 mL 3-necked flask, then 15 mL of OA and 30 mL of ODE were added. Under a nitrogen flow, the flask was heated to 160 °C and kept for 1 h with vigorous stirring. After natural cooling, a 10 mL methanol solution containing 8 mmol of NH_4F and 5 mmol of NaOH was added dropwise. The resulting solution was stirred at room temperature for 2 h and heated to 70 °C until all methanol evaporated. The solution was then heated to 290 °C and kept for 1.5 h under a gentle flow of nitrogen. After natural cooling, the nanocrystals were precipitated by adding 50 mL of ethanol. After being collected by centrifugation (10,000 rpm, 15 min), they were washed with water and then with a mixture of cyclohexane and ethanol (1:10, v/v), and finally stored as dispersion in 10 mL of cyclohexane.

$NaYF_4$ shell precursor was prepared by heating a mixture of 0.8 mmol of $YCl_3 \cdot 6H_2O$, 15 mL of OA and 30 of mL ODE in a 100 mL 3-necked flask to 160 °C under nitrogen flow and kept for 30 min. The solution was then cooled to room temperature. 1 mmol of core nanoparticles in 5 mL of cyclohexane was added into the solution and sonicated for 30 min. The flask was heated to 90 °C to remove cyclohexane, and then was cooled to room temperature. 5 mL of methanol solution containing 1 mmol of NH_4F and 1.7 of mmol NaOH was added dropwise with vigorous stirring for 2 h. After evaporating the methanol at 70 °C, the mixture was heated to 290 °C for 1.5 h under nitrogen flow. After cooling, the nanoparticles were precipitated and washed following the identical procedure mentioned above.

2.4. Synthesis of mesoporous silica coated upconversion nanoparticles (UCNPs@$mSiO_2$)

The preapration of UCNPs@$mSiO_2$ followed a reported procedure with some modifications (Sun et al., 2013). In details, 5 mL of cyclohexane containing 20 mg of UCNPs was added along with 0.1 g of cetyltrimethylammonium bromide (CTAB) into 50 mL of deionized water to form an oil-in-water emulsion. The mixture was stirred vigorously for 1 h, then was heated to 85 °C to remove cyclohexane. The dispersion was diluted with 100 mL of water, and then 0.2 mL of hydrazine (80%) was added. The flask was then sealed and stirred for 1 h. 100 μL of tetraethyl orthosilicate (TEOS) was delivered into the flask dropwise before the mixture was heated to 80 °C and kept for 2 h under vigorous stirring. The particles were collected by centrifugation and washed with ethanol for three times.

The collected product was extracted for 3 h in a 6 g L^{-1} of ethanol solution of ammonium nitrate (NH_4NO_3) at 60 °C. This procedure was repeated twice to remove template reagent CTAB.

2.5. Synthesis of Probe 1

Operations mentioned in this section were taken in a dark room. Aluminum foil was used as a cover.

0.5 g of 5(6)-carboxyfluorescein was dispersed in 10 mL of anhydrous CH_2Cl_2, 0.67 g of Et_3N was then added at 0 °C. After being

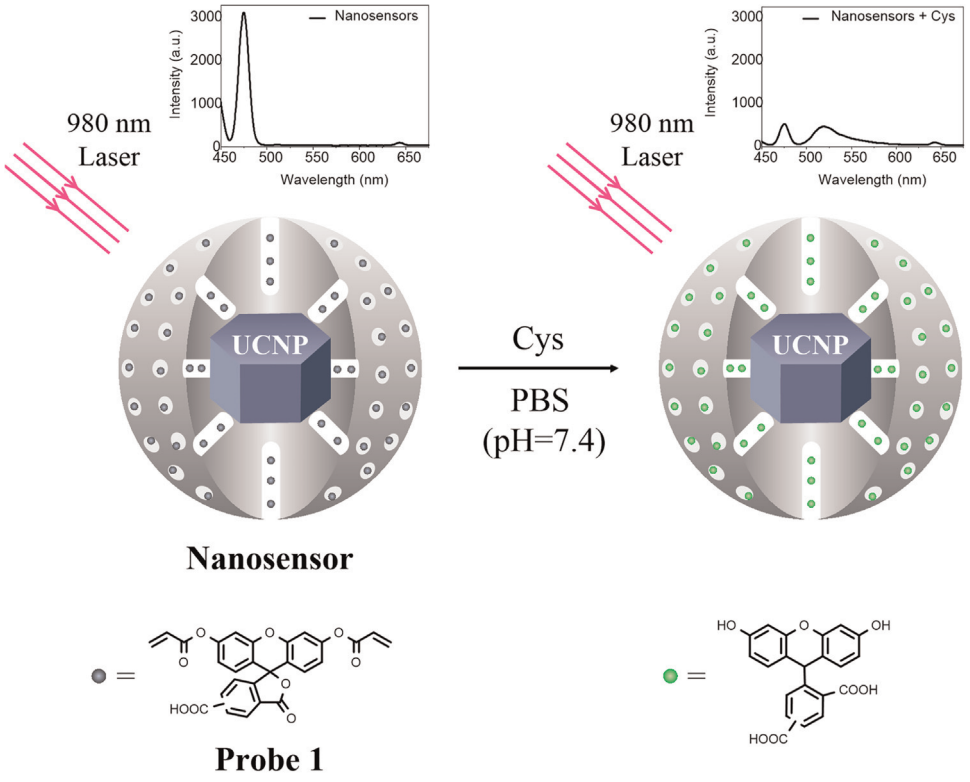

Fig. 1. Illustration of the nanosensor and the sensing process. (For interpretation of the references to color in this figure, the reader is referred to the web version of this article.)

stirred for 30 min, 0.6 g of acryloyl chloride was added dropwise. The mixture was sealed and stirred at 0 °C for 1 h and then at room temperature overnight. The resulting solution was washed with water to remove excess reactants. After being dried with magnesium sulfate anhydrous, the solution was evaporated. Crude product was purified by silica gel column chromatography using CH_2Cl_2:CH_3OH (50:1) as eluent to afford 0.4 g of product (yield 62%). 5- and 6- carboxyl isomers could not be separated from each other, and Probe 1 was a mixture of these two isomers (Scheme S1, Supplementary material).

Probe 1: ^{1}H NMR ($CDCl_3$, 300 MHz) δ (ppm): 6.08 (4H, dd, J_1 = 1.1 Hz, J_2 = 10.6 Hz, –CH=CHH); 6.33 (4H, dd, J_1 = 10.6 Hz, J_2 = 17.6 Hz, –CH=CHH); 6.65 (4 H, dd, J_1 = 1.1 Hz, J_2 = 17.2 Hz, –CH=CHH); 6.83–6.92 (8H, m, upper-ring Ar–H); 7.19 (4H, upper-ring Ar–H)*; 7.33 (1H, d, J = 8.1 Hz, lower-ring Ar–H); 7.92 (1H, s, lower-ring Ar–H); 8.15 (1H, d, J = 8.1 Hz, lower-ring Ar–H); 8.36–8.43 (2H, m, lower-ring Ar–H); 8.78 (1H, s, lower-ring Ar–H).**

*Several peaks with very similar chemical shifts (within 4 Hz) overlapped.

**Peaks from carboxyl groups were not observed on this spectrum.

2.6. Preparation of the nanosensors

To load **Probe 1** into the channels of UCNPs@mSiO_2, 10 mL of ethanol dispersion containing 20 mg of UCNPs@mSiO_2 was mixed with 20 mg of **Probe 1**. The mixture was sonicated for 1 h and then evaporated under reduced pressure. Disperse–sonicate–evaporate process was repeated twice before the residuum was washed with ethanol. The loaded nanosensors were then collected by centrifugation. For further measurement, they were dispersed in 20 mL of water and stored in darkness at 4 °C.

2.7. Detection of Cys

In a typical run, the nanosensors were dispersed with a final concentration of 0.25 mg mL^{-1} in PBS (pH=7.4), photoluminescence measurement was taken 10 min after analyte was injected. Samples were excited by 980 nm CW laser at a power density of ~100 W cm^{-2}.

2.8. Detection of Cys in human serum

HPLC experiments were carried at room temperature with acetonitrile: 0.1% acetic acid solution (5: 95, v/v) as mobil phase. Human serum was diluted with HPLC grade water for 10 times before delivered. 1 mmol L^{-1} (mM) of Cys solution was used as standard to draw a characteristic curve with which the Cys concentration in human serum was able to be calculated.

For detection using the nanosensors, 20 μL of human serum was diluted to 2 mL with PBS (pH=7.4) containing 0.25 mg mL^{-1} of nanosensors. A 980 nm CW laser with power density of ~100 W cm^{-2} was used as exciting source.

3. Results and discussion

3.1. Design of the nanosensors

Probe 1, a carboxyfluorescein-based derivate that can selectively react with Cys was synthesized. To ratiometricly detect Cys, a system combined with UCNPs, mesoporous silica and **Probe 1** was established. Tm^{3+} doped UCNPs with optimized size and coating were chosen according to reported articles (Liu et al. 2014; Shi et al. 2011) as energy donor. **Probe 1** was loaded in mesopores of silica physically. Although **Probe 1** will diffuse out from pores unavoidably, it absorbs blue light from UCNPs initiated by NIR

laser and emits green light upon addition of Cys. Being treated with different concentrations of Cys, intensities of the green and blue lights will change ratiometricly in a certain range, which makes the system an effective sensor for detecting Cys. Demonstration of the sensing process was depicted in Fig. 1.

3.2. Preparation and characterization

Core–shell UCNPs were synthesized through thermal decomposition. The atomic ratio of Y:Yb:Tm in $NaREF_4$ core was designed as 79.5:20:0.5; the shell was composed of $NaYF_4$ without doping. Their XRD patterns (Fig. S1, Supplementary material) indicate that both the core and the core–shell structured nanocrystals are hexagonal-phase (JCPDS 28-1192). There is a ~0.12 degree of decrease of full width at half maxima (FWHM) for each peak of core–shell particles, suggesting that their average size is a little bigger than that of uncoated core. The approximate atomic ratio of Y to Yb obtained by EDS is 74:26 for the core and 85:15 for the core–shell UCNPs, respectively (Fig. S2, Supplementary material). The increase in Y element can be assigned to $NaYF_4$ coating. Mesoporous silica coated nanoparticles UCNPs@$mSiO_2$ was synthesized following a one-step emulsion method (Sun et al., 2013). CTAB was used here as an emulsifier and template reagent. Fig. S3 shows TEM images of UCNPs@$mSiO_2$. Mean diameter of UCNPs@$mSiO_2$ particles is around 75–80 nm, with thickness of mesoporous silica shell ~20 nm.

5(6)-Carboxyfluorescein contains a carboxyl group off No. 5 or 6 carbon on fluorescein's lower-ring structure. The 5- and 6- isomers are virtually identical in reactivity and fluorescent characteristics (Hermanson 2008). For **Probe 1**, these two isomers were not separated since they owned the same retention time and could not be separated by gel column chromatography method. Their ^1H NMR spectrum (Fig. S4, Supplementary material) shows that peaks from acroloyl groups of two isomers totally overlap with each other, and peaks from upper-ring of fluorescein have very close chemical shifts. The distinction between protons on the lower-ring of two isomers is relatively obvious. Corresponding integration result indicates that 5- and 6- isomers are mixed approximately in an equal proportion.

Nitrogen adsorption–desorption isotherms (Fig. S5, Supplementary material) show that the adsorption capacity of the nanosensors is lower than that of unloaded UCNPs@$mSiO_2$. Decreases of the BET surface area from 428.6 $m^2\,g^{-1}$ for UCNPs@$mSiO_2$ to 408.3 $m^2\,g^{-1}$ for the nanosensors and calculated volume of pores from 0.647 $cm^3\,g^{-1}$ to 0.576 $cm^3\,g^{-1}$ were observed (Table S1, Supplementary material) suggesting **Probe 1** was successfully loaded into mesopores.

3.3. Cys detection

The nanosensors were applied to detection of Cys in aqueous solution (PBS, pH=7.4). According to the emission spectrum of UCNPs excited by 980 nm NIR laser and emission spectra of **Probe 1** before and after being treated with Cys (Fig. S6, Supplementary material), **Probe 1** has little absorbance in region of 400–550 nm and is practically non-fluorescent in visible region. In other words, it hardly absorbs the blue emission assigned to $^1G_4 \rightarrow {}^3H_6$ transition of Tm^{3+} from UCNPs. After being treated with Cys, **Probe 1** will be transformed to substances with intense green fluorescence and absorbance overlapping with the blue UC emission. As illustrated in Fig. 2(A), the UC luminescence of Tm^{3+} at 475 nm is gradually decreased, while the emission of carboxyfluorescein at 518 nm increases with increasing Cys concentrations. On the other hand, the red emission centering at 643 nm corresponding to $^1G_4 \rightarrow {}^3F_4$ transition of Tm^{3+} is well preserved.

In a fluorescent detection, signals from only one single emission band are considered unreliable unless all external factors are

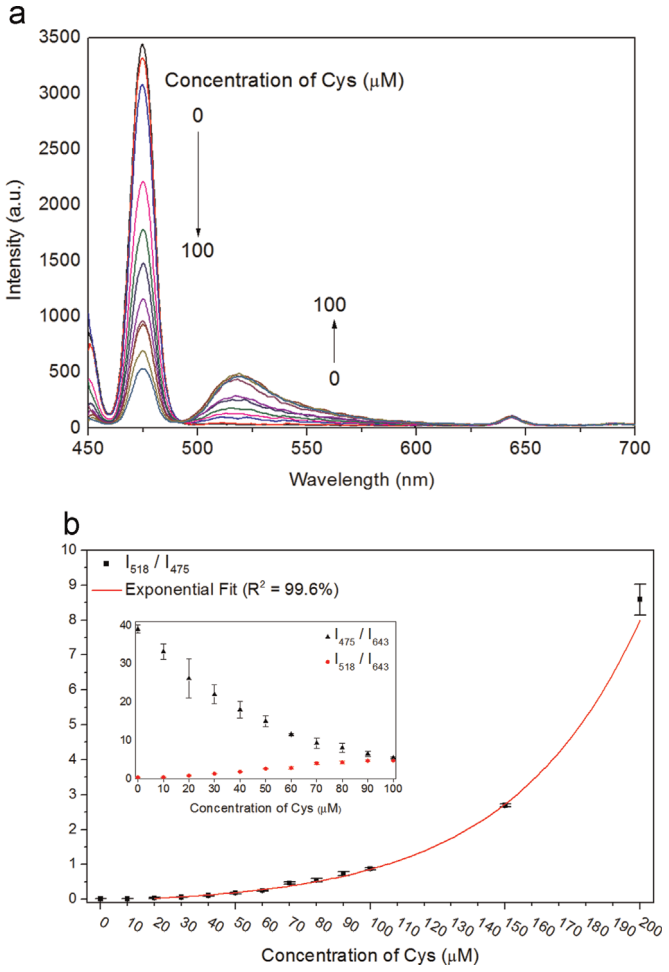

Fig. 2. (A) Fluorescence spectra of the nanosensors + Cys in PBS (pH = 7.4). (B) Plots of fluorescence response I_{518}/I_{475} of the nanosensors treated with increasing amount of Cys from 0 to 200 μM in PBS (pH = 7.4), and I_{518}/I_{643} and I_{475}/I_{643} respectively upon addition of Cys from 0 to 100 μM (inner). Detecting system was driven by a 980 nm CW laser.

severely restricted which is almost impossible in practical operations. Therefore internal references are critical to get reliable signals. As the red emission of Tm^{3+} at 643 nm is not affected by either carboxyfluorescein or Cys, it is here used as an internal reference to investigate the variation of blue emission from Tm^{3+} at 475 nm and green emission from carboxyfluorescein at 518 nm. As shown in Fig. 2 (B), the intensity ratio between bands at 475 nm and 643 nm (I_{475}/I_{643}) decreases exponentially, while the ratio I_{518}/I_{643} increases linearly when Cys concentration increases from 10 to 100 μmol L^{-1} (μM). The ratio I_{518}/I_{475} is fitted well in exponential growth with an equation of $I_{518}/I_{475} = 0.1314 \cdot \exp(c_{(Cys)}/48.42) - 0.1775$ ($R^2 = 99.6\%$), where $c_{(Cys)}$ is the concentration of Cys (μM). With this regression equation, Cys levels in samples can be calculated from UC emission spectra in an effective range from 20 to 200 μM. The limit of detection (LOD) for Cys which is defined as signal-to-noise(S/N) ratio = 3 is calculated as 20 μM. Comparison of sensing performance of the nanosensors with some other previous works was listed in Table 1 demonstrating the nanosensors in this work had wide measurement range.

Response time is critical to chemical sensors, especially for biosamples whose analyte levels may vary through biological processes. Time scan was thus taken to investigate the response time. After mixing Cys (50 μM) with the nanosensors (0.25 mg mL^{-1}), the intensity of UC emission at 475 nm decreased exponentially

Table 1
Performance comparison of the performance of several Cys sensors.

Sensors	Limit of detection (μM)	Measurement range (μM)	References
CY-NB	0.2	0.2–100	Yin et al. (2015)
NRFTP	0.082	10–100	Long et al. (2011)
Fluorescein acrylate	0.5	2–25	Wang et al. (2012b)
YSUCNP-ANP	28.5	0–18 equiv.	Zhao et al. (2014)
ACA	0.657	0.657–40	Dai et al. (2014)
PEO-Py/Au NPs	0.0114	0.0125–0.225	Xu et al. (2010)
HMBT derivate	0.11	0.11–40	Yang et al. (2011)
UCNPs@mSiO2 loading **Probe 1**	20	20–200	This work

with a half-life ($t_{1/2}$) of 100 s (Fig. S7, Supplementary material) and became constant after ~10 min. Thus all nanosensor-employed samples were held for 10 min before fluorescent measurement.

3.4. Mechanism of ratio fluorescence

For a better understanding on the energy transfer mechanism, emission decay dynamics were studied (Fig. S8, Supplementary material). It is observed that luminescence decays of unloaded UCNPs@mSiO$_2$ and the nanosensors upon addition of Cys at 475 nm fit mono-exponential decay well with lifetimes of 829 μs (R^2=99.3%) and 811 μs (R^2=99.2%), respectively. It is only a slight difference between the two samples, suggesting that the dominant energy transfer mechanism should be emission–reabsorption rather than Förster resonance energy transfer (Zhang et al., 2012).

It was reported that the cleavage of acrylic ester under Cys treatment was very efficient because of the high nucleophilicity of thiol group and the tendency to form a 7-membered ring (Wang et al., 2012a). As a consequence, it is rationally presumed that the intensity of fluorescence from carboxyfluorescein at 518 nm is proportional to Cys concentration at unsaturated levels, resulting in the linear relationship between $c_{(Cys)}$ and I_{518}/I_{643}.

The Beer–Lambert law has been described as follows:

$$A = \lg\left(\frac{I_0}{I}\right) = \varepsilon \ell c$$

Where A is the absorbance of carboxyfluorescein at 475 nm; I_0 is the intensity of UC emission at 475 nm before Cys treatment; I is the intensity of UC emission at 475 nm after Cys treatment; c is the concentration of carboxyflurescein coming from **Probe 1** reacting with Cys, respectively. The concentration of carboxyfluorescein changes linearly with that of Cys in the nanosensors' working range, and the recorded exponential decay of UC emission at 475 nm along with increasing concentration of Cys fits the Beer–Lambert law, which further confirm that the UC luminescence at 475 nm is quenched and green luminescence at 518 nm is excited via an emission–reabsorption process.

3.5. Selectivity of the nanosensors

Selectivity of the nanosensors is tested as follows. Glycine (Gly), aspartic acid (Asp) and methionine (Met) are chosen as representatives of amino acids. Thioglycolic acid (TGA), GSH and Hcy are chosen for their thiol-based nucleophilicities which are similar to Cys. These samples are tested under identical condition where the nanosensors were dispersed in PBS (pH=7.4) at a level of 0.25 mg mL^{-1} with analyt concentration of 50 μM. The ratiometric fluorescent response of the nanosensors to each analyte is illustrated in Fig. 3, an effective specificity for Cys is observed. The intensity ratio I_{518}/I_{475} is 0.011 for blank measurement (relative standard deviation, RSD=4.9%), 0.014 for Gly (RSD=5.4%), 0.014 for Asp (RSD=5.3%), 0.12 for Met (RSD=3.8%), 0.048 for TGA (RSD=3.4%), 0.021 for GSH (RSD=2.9%), 0.020 for Hcy (RSD=5.0%)

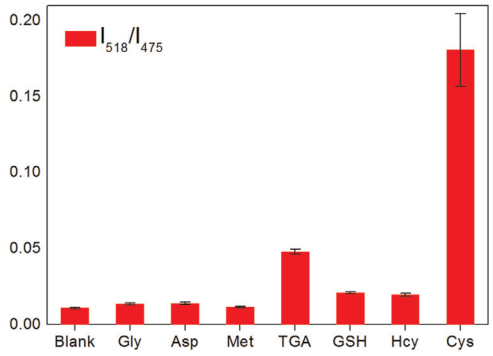

Fig. 3. Fluorescence responses of the nanosensors towards analytes including Gly, Asp, Met, TGA, GSH, Hcy and Cys. (λ_{ex}=980 nm).

and 0.181 for Cys (RSD=13.2%) respectively. Among these analytes, only TGA has obvious effect on the nanosensors at this interference concentration.

Ratiometric change of two emission bands in one system leads to its color change of luminescence. For most circumstances, it is easier to recognize a color change than a brightness change with naked eyes. Photographs of UC luminescence taken by a digital camera are illustrated in Fig. 4, demonstrating the luminescence color change of the nanosensors. Luminescence color is hardly influenced by GSH and Hcy. After being treated with Cys, luminescence color varies from royal blue to pale green.

For the reaction between acrylates and Cys/Hcy, an addition-and-cyclization presumption has been proposed (Scheme S2, Supplementary material) (Wang et al., 2012a; Yang et al., 2011). In this paper, the results of sensing assay suggest that **Probe 1** is more sensitive to Cys. It is worth to notice that all these amino acids and TGA in this assay would entail fluorescence recovery of fluorescein given reaction time long enough, overnight for instance. Generally, amino and thiol groups are more nucleophilic than hydroxyl group, which means that acrylates will be amidated or thioesterified finally. In other words, the selectivity is under kinetic control and thus meaningful only in a certain period of time. In above assays, the nanosensors' specificity towards Cys lasts several hours which entitles it to sufficient practicality.

It is assumed that the reaction between fluorescein-O,O′-diacrylate and Cys is more efficient because the 7-membered ring Cys addition-and-cyclization product is thermodynamically more stable than 8-membered ring Hcy counterpart. In this report, improved selectivity is attributed to the 5- or 6-carboxyl group off the lower ring of fluorescein as well. The intramolecular hydrogen bond is supposed as another factor that keeps Hcy addition product from cyclization.

To confirm this assumption, DFT calculation is performed on the products of Hcy and **Probe 1** at RB3LYP/6-311 G(d,p) level. As mentioned before, the cleavage of acrylates results from the cyclization of Cys/Hcy addition intermediates. An amino group (–NH_2) and a carboxyl group (–COOH) exist on the chain of thiol-

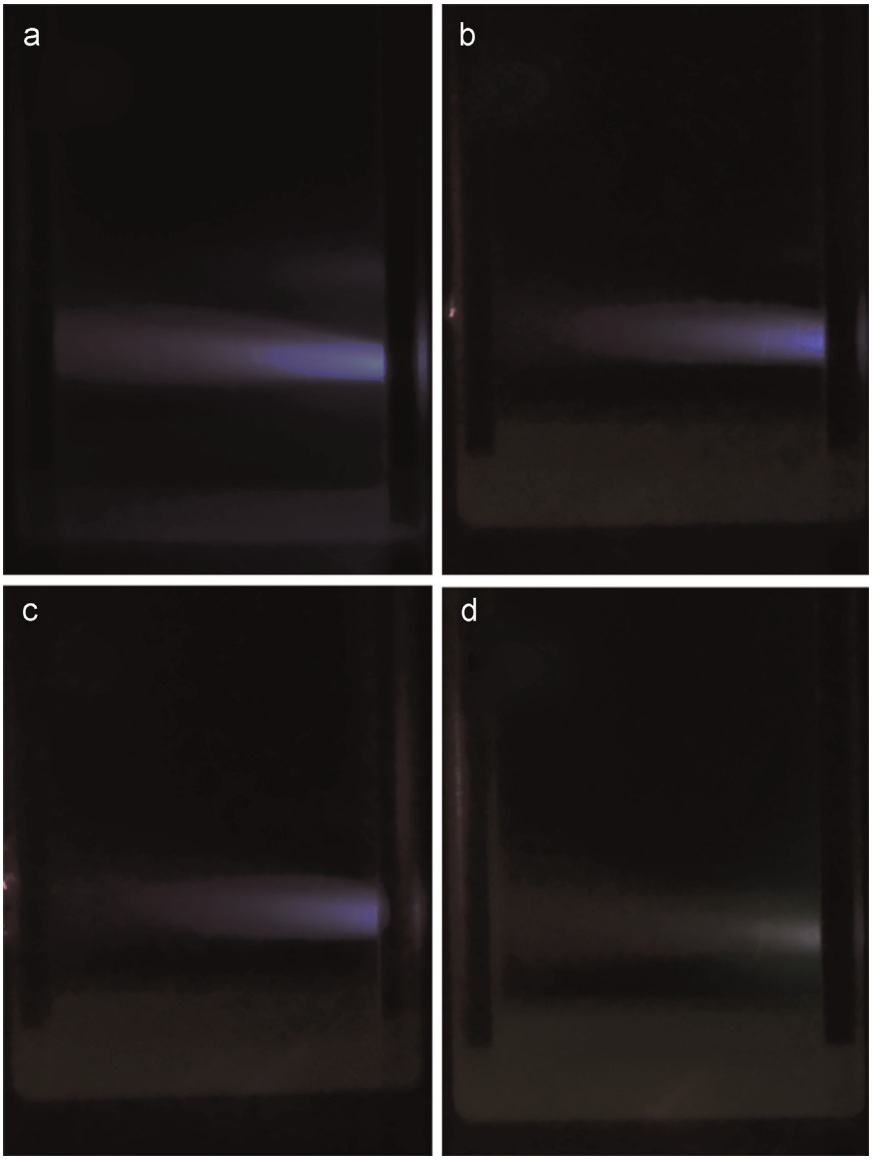

Fig. 4. Photographs of UC luminescnce of the nanosensors (0.25 mg mL^{-1} in PBS) (a) and them upon addition of 50 μM of GSH (b), Hcy (c) and Cys (d). 980 nm CW laser was used as the excitation source. (For interpretation of the references to color in this figure, the reader is referred to the web version of this article.)

contained amino acids added on **Probe 1**. For Cys, the $-NH_2$ is capable of attacking acrylate easily to form a 7-membered ring. For Hcy, however, the upcoming 8-menbered ring strain keeps the $-NH_2$ away from the acrylate group. The length of Hcy molecule is just right that enables the $-NH_2$ and –COOH end to get close enough to the carboxyl group off the lower ring of fluorescein moiety (Fig. S9d and e, Supplementary material), making the intramolecular hydrogen bond possible. Optimized geometric structures illustrate that the distance between $-NH_2$ of Hcy and 5-carboxyl group of fluorescein is 3.52 Å (Fig. S9b, Supplementary material) which is relatively longer than that between $-NH_2$ of Hcy and 6-carboxyl group (1.74 Å) and that between –COOH of Hcy and 6-carboxyl group (1.91 Å). The atom distances in the 6-carboxyl model coincide with typical O–H···N and O–H···O hydrogen bonds length, confirming the existence of intramolecular hydrogen-bond-like interactions (Desiraju 2002). In the 5-carboxyl model, on the other hand, calculation result tentatively denys the possibility of such intramolecular interaction. These interactions are expected to cooperate with the ring strain factor to keep Hcy from turning **Probe 1** on, resulting in selective sensing for Cys.

3.6. Detection of Cys in human serum

To evaluate the sensing performance of the nanosensors towards real bio-sample, they were employed to detect Cys in diluted human serum. By converting the luminescence intensity ratio (Fig. S10. Supplementary material) to concentration using the characteristic equation, Cys in serum was found to be 152 ± 2 μM in 100 times diluted serum which means that Cys concentration in original serum sample was 15.2 ± 0.2 mM. By comparison, HPLC analysis was carried as standard. Concentration of Cys in human serum sample was found to be 13.23 mM (Fig. S11. Supplementary material). These results are listed in Table 2. It is possible that the nanosensors were interfered by some bio-molecules triggering false-positive, which explains the fact that Cys level measured by them is higher than it by means of HPLC. Abnormal concentration that much higher than reported healthy range (Wang et al., 2005) may result from hydrolysis of protein and peptide in serum caused by improper sample transport or storage.

Table 2
Detection of Cys in human serum.

Concentration of Cys in human serum (mM)		Recovery (%)
Nanosensors	HPLC	
15.2 ± 0.2	13.23	114.9 ± 1.5

4. Conclusions

A prototype of nanosensors based on UC luminescence for Cys detecting was prepared in this work. The nanosensor was constructed with a UCNP core, a layer of mesoporous silica shell and fluorescein-based **Probe 1** loaded in the channels of silica. The UC luminescence at 475 nm driven by 980 nm NIR laser in turn excited **Probe 1** to give green emission at 518 nm upon addition of Cys. With a well fitted regression equation, Cys concentration is expected to be calculated from a luminescence intensity ratio I_{518}/I_{475}. The nanosensors exhibited a kinetically-controlled selectivity and were able to distinguish Cys from Hcy and GSH. The response of the nanosensors towards Cys was also recognizable with naked eyes by color change of luminescence. The mechanism of the ratiometric fluorescence was proved as emission–reabsorption by lifetime comparison. The system was capable of detecting Cys in human serum as well. Overall, our results present a promising strategy for constructing nanosensors of quick response, ease of fabrication and good selectivity to detect Cys in aqueous solution.

Acknowledgment

The authors gratefully thank the financial supports of the NSFC (Grant nos. 51572256, 51172224 and 51372240) and the Science and Technology Developing Project of Jilin Province (Grant no. 201201009).

Appendix A. Supplementary material

Supplementary data associated with this article can be found in the online version at http://dx.doi.org/10.1016/j.bios.2015.09.034.

References

Chen, X., Zhou, Y., Peng, X., Yoon, J., 2010. Fluorescent and colorimetric probes for detection of thiols. Chem. Soc. Rev. 39 (6), 2120–2135.
Dai, X., Wu, Q.-H., Wang, P.-C., Tian, J., Xu, Y., Wang, S.-Q., Miao, J.-Y., Zhao, B.-X., 2014. A simple and effective coumarin-based fluorescent probe for cysteine. Biosens. Bioelectron. 59, 35–39.
Desiraju, G.R., 2002. Hydrogen bridges in crystal engineering: interactions without borders. Acc. Chem. Res. 35 (7), 565–573.
Ding, Y., Zhu, H., Zhang, X., Zhu, J.J., Burda, C., 2013. Rhodamine B derivative-functionalized upconversion nanoparticles for FRET-based Fe(3+)-sensing. Chem. Commun. 49 (71), 7797–7799.
Hermanson, G.T., 2008. Bioconjugate Techniques, 2nd edition. Elsevier Inc, Amsterdam.
Levine, J., Timinsky, I., Vishne, T., Dwolatzky, T., Roitman, S., Kaplan, Z., Kotler, M., Sela, B.A., Spivak, B., 2008. Elevated serum homocysteine levels in male patients with PTSD. Depression Anxiety 25 (11), E154–E157.
Li, C., Liu, J., Alonso, S., Li, F., Zhang, Y., 2012. Upconversion nanoparticles for sensitive and in-depth detection of Cu2+ ions. Nanoscale 4 (19), 6065–6071.
Li, X., Wu, Y., Liu, Y., Zou, X., Yao, L., Li, F., Feng, W., 2014. Cyclometallated ruthenium complex-modified upconversion nanophosphors for selective detection of Hg2+ ions in water. Nanoscale 6 (2), 1020–1028.
Liu, J., Liu, Y., Bu, W., Bu, J., Sun, Y., Du, J., Shi, J., 2014. Ultrasensitive nanosensors based on upconversion nanoparticles for selective hypoxia imaging in vivo upon near-infrared excitation. J. Am. Chem. Soc. 136 (27), 9701–9709.
Liu, J., Liu, Y., Liu, Q., Li, C., Sun, L., Li, F., 2011. Iridium(III) complex-coated nanosystem for ratiometric upconversion luminescence bioimaging of cyanide anions. J. Am. Chem. Soc. 133 (39), 15276–15279.
Long, L., Lin, W., Chen, B., Gao, W., Yuan, L., 2011. Construction of a FRET-based ratiometric fluorescent thiol probe. Chem. Commun. 47 (3), 893–895.
Peng, H., Chen, W., Cheng, Y., Hakuna, L., Strongin, R., Wang, B., 2012. Thiol reactive probes and chemosensors. Sensors 12 (11), 15907–15946.
Reddie, K.G., Carroll, K.S., 2008. Expanding the functional diversity of proteins through cysteine oxidation. Curr. Opin. Chem. Biol. 12 (6), 746–754.
Seshadri, S., Beiser, A., Selhub, J., Jacques, P.F., Rosenberg, I.H., D'Agostino, R.B., Wilson, P.W.F., Wolf, P.A., 2002. Plasma homocysteine as a risk factor for dementia and Alzheimer's disease. New Engl. J. Med. 346 (7), 476–483.
Shahrokhian, S., 2001. Lead phthalocyanine as a selective carrier for preparation of a cysteine-selective electrode. Anal. Chem. 73 (24), 5972–5978.
Shi, F., Wang, J., Zhang, D., Qin, G., Qin, W., 2011. Greatly enhanced size-tunable ultraviolet upconversion luminescence of monodisperse β-NaYF4:Yb,Tm nanocrystals. J. Mater. Chem. 21 (35), 13413.
Sun, L., Liu, T., Qiu, Y., Liu, J., Shi, L., Wolfbeis, O.S., 2013. Direct formation of mesoporous upconverting core-shell nanoparticles for bioimaging of living cells. Microchim. Acta 181 (7–8), 775–781.
Wald, D.S., Law, M., Morris, J.K., 2002. Homocysteine and cardiovascular disease: evidence on causality from a meta-analysis. Br. Med. J. 325 (7374), 1202.
Wang, H., Zhou, G., Gai, H., Chen, X., 2012a. A fluorescein-based probe with high selectivity to cysteine over homocysteine and glutathione. Chem. Commun. 48 (67), 8341–8343.
Wang, L., Zhou, Q., Zhu, B., Yan, L., Ma, Z., Du, B., Zhang, X., 2012b. A colorimetric and fluorescent chemodosimeter for discriminative and simultaneous quantification of cysteine and homocysteine. Dyes Pigment. 95 (2), 275–279.
Wang, W., Rusin, O., Xu, X., Kim, K.K., Escobedo, J.O., Fakayode, S.O., Fletcher, K.A., Lowry, M., Schowalter, C.M., Lawrence, C.M., Fronczek, F.R., Warner, I.M., Strongin, R.M., 2005. Detection of homocysteine and cysteine. J. Am. Chem. Soc. 127 (45), 15949–15958.
Weerapana, E., Wang, C., Simon, G.M., Richter, F., Khare, S., Dillon, M.B., Bachovchin, D.A., Mowen, K., Baker, D., Cravatt, B.F., 2010. Quantitative reactivity profiling predicts functional cysteines in proteomes. Nature 468 (7325), 790–795.
Xu, J.P., Jia, L., Fang, Y., Lv, L.P., Song, Z.G., Ji, J., 2010. Highly soluble PEGylated pyrene-gold nanoparticles dyads for sensitive turn-on fluorescent detection of biothiols. Analyst 135 (9), 2323–2327.
Yang, X., Guo, Y., Strongin, R.M., 2011. Conjugate addition/cyclization sequence enables selective and simultaneous fluorescence detection of cysteine and homocysteine. Angew. Chem. 50 (45), 10690–10693.
Yao, L., Zhou, J., Liu, J., Feng, W., Li, F., 2012. Iridium-complex-modified upconversion nanophosphors for effective LRET detection of cyanide anions in pure water. Adv. Funct. Mater. 22 (13), 2667–2672.
Yin, K., Yu, F., Zhang, W., Chen, L., 2015. A near-infrared ratiometric fluorescent probe for cysteine detection over glutathione indicating mitochondrial oxidative stress in vivo. Biosens. Bioelectron. 74, 156–164.
Yuan, L., Lin, W., Yang, Y., 2011. A ratiometric fluorescent probe for specific detection of cysteine over homocysteine and glutathione based on the drastic distinction in the kinetic profiles. Chem. Commun. 47 (22), 6275–6277.
Yuan, L., Lin, W., Zheng, K., Zhu, S., 2013. FRET-Based small-molecule fluorescent probes: rational design and bioimaging applications. Acc. Chem. Res. 46 (7), 1462–1473.
Zhang, J., Li, B., Zhang, L., Jiang, H., 2012. An optical sensor for Cu(II) detection with upconverting luminescent nanoparticles as an excitation source. Chem. Commun. 48 (40), 4860–4862.
Zhang, J., Li, B., Zhang, L., Zhang, L., 2013. An optical probe possessing upconversion luminescence and Hg(2+)-sensing properties. Chemphyschem 14 (13), 2897–2901.
Zhao, L., Peng, J., Chen, M., Liu, Y., Yao, L., Feng, W., Li, F., 2014. Yolk-shell upconversion nanocomposites for LRET sensing of cysteine/homocysteine. ACS Appl. Mater. Interfaces 6 (14), 11190–11197.